IEEE Photonics Journal
An IEEE Photonics Society Publication

Open Access

High-Power and High-Efficiency 1.3-μm Superluminescent Diode With Flat-Top and Ultrawide Emission Bandwidth

Volume 7, Number 1, February 2015

M. Z. M. Khan, Member, IEEE
H. H. Alhashim
T. K. Ng, Member, IEEE
B. S. Ooi, Senior Member, IEEE

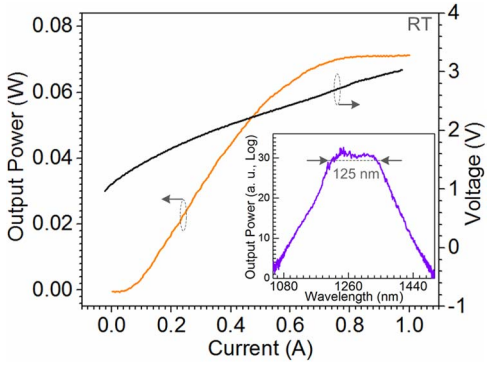

DOI: 10.1109/JPHOT.2015.2399442
1943-0655 © 2015 IEEE

High-Power and High-Efficiency 1.3-μm Superluminescent Diode With Flat-Top and Ultrawide Emission Bandwidth

M. Z. M. Khan, *Member, IEEE*, H. H. Alhashim, T. K. Ng, *Member, IEEE*, and B. S. Ooi, *Senior Member, IEEE*

Photonics Laboratory, Computer, Electrical and Mathematical Science and Engineering (CEMSE) Division, King Abdullah University of Science & Technology (KAUST), Thuwal 23955-6900, Saudi Arabia

DOI: 10.1109/JPHOT.2015.2399442

Manuscript received January 11, 2015; revised January 28, 2015; accepted January 28, 2015. Date of publication February 4, 2015; date of current version February 18, 2015. This work was supported by King Abdullah University of Science and Technology under its baseline funding and Competitive Research Grant CRG-1-2012-OOI-010. Corresponding author: B. S. Ooi (e-mail: boon.ooi@kaust.edu.sa).

Abstract: We report on a flat-top and ultrawide emission bandwidth of 125 nm from InGaAsP/InP multiple quantum-well (MQW) superluminescent diode with antireflection coated and tilted ridge-waveguide device configuration. A total output power in excess of 70 mW with an average power spectral density of 0.56 mW/nm and spectral ripple $\leq 1.2 \pm 0.5$ dB is measured from the device. Wall-plug efficiency and output power as high as 14% and 80 mW, respectively, is demonstrated from this batch of devices. We attribute the broad emission to the inherent inhomogeneity of the electron–heavy-hole (e-hh) and electron–light-hole (e-lh) recombination of the ground state and the first excited state of the MQWs and their simultaneous emission.

Index Terms: Multiple quantum-wells, superluminescent diode, high-power, broadband emission, inhomogeneous broadening.

1. Introduction

High power and broadband superluminescent diode (SLD) with flat-top emission spectrum is a desirable optical source in noninvasive biomedical imaging techniques employing low coherence interferometry, for instance, optical coherence tomography (OCT) [1]. Several broadband SLDs have been reported for OCT applications, encompassing emission wavelength ~1000 nm [2], [3], ~1300 nm [4]–[11] and ~1500 nm [12]–[14], and using different quantum confined nanostructure based active regions, ranging from quantum-wells (QW) [7]–[12] to quantum dots (Qdots) [3]–[6], and very recently quasi-zero dimensional quantum dashes [13], [14]. For the ~1300 nm wavelength window, active region designs based on both multi-stack Qdots and MQW nanostructures have been investigated. In the design of Qdots based SLDs, both identical and chirped multi-stack InAs/GaAs active region have been demonstrated. Moreover, intermixing and p-doping techniques were also employed to extend the Qdot SLD emission bandwidth and device performance [4]. In general, output power in tens-of-milliwatts up to ~180 mW, and emission bandwidth (−3 dB) in tens of nm to ~310 nm, have been achieved, and very recently reaching ~350 nm via simultaneous emission from hybrid QW-Qdot active region [5], [15]. As

for the conventional ~1300 nm QW-based SLDs, high power of >100 mW has been reported with optical bandwidth reaching several tens of nanometers to about 100 nm [7]–[11]. The improvement in the SLD figures of merit, such as optical power, large spectral bandwidth, and flat-top spectral shape are required for achieving higher axial resolution, improved signal-to-noise ratio, and penetration depth in an OCT system. However, simultaneous optimization of power and bandwidth [i.e., power-bandwidth product (PBP)] still pose a challenge in both types of active regions. In the MQW domain, various research paths have been explored and demonstrated to optimize PBP and spectral profile in particular. For instance, by employing (a) identical MQWs active region and relying on simultaneous emission from QWs ground state (GS) and first excited state (ES) [10], [16]; (b) asymmetric MQWs based on simultaneous GS emissions [7], [8]; and (c) combination of both the above approaches [17]. In general, the method in (a) usually results in spectral dip in the amplified spontaneous emission (ASE) spectrum which affects the OCT resolution and usable power [4], while both approaches in (b) and (c) require comparatively complex and optimized epitaxial structure design. SLD with ultra-wide emission bandwidth of > 250 nm, centered at ~1450 nm, have been reported based on approach (c), however, with a very lower output power of ~0.2 mW [17].

In this work, a simpler identical MQW epitaxial structure is utilized. By properly engineering the GS and ES e-hh and e-lh emission overlaps of each QW states with comparable emission intensities across the inhomogeneous optical transitions, in a compressively strained four QW active region; we demonstrate a SLD with simultaneous achievement of wide and flat-topped 125 nm optical bandwidth and output power of 70 mW, which corresponds to a PBP of 8750 mWnm. This value is better than the commercially available pigtailed SLDs encompassing ~1300 nm wavelength, with exhibited PBP value in the range of 300–1650 mWnm [18]–[20]. Moreover, wall-plug efficiency (WPE) in excess of 14% is demonstrated from this batch of devices while preserving the device performance. This is attributed to the variation in anti-reflection (AR) coating properties, which can be applied as a facet engineering technique to enhance PBP of SLDs. The WPE and optical bandwidth values, to our knowledge, are the best values reported at ~1300 nm wavelength window. Besides addressing the field of biomedical imaging, optical short reach communications, such high-power and broadband near infra-red SLD devices could serve as key sources in optical time domain reflectometry, fiber gyroscopes, etc., thus improving the respective system's performance characteristics [5], [14].

2. Experimental Method

The device active region consists of four 6.7 nm thick compressively strained $InGa_{0.84}As_{0.59}P$ QWs separated by 10 nm thick tensile strained $InGa_{0.863}As_{0.255}P$ barrier layers. The un-doped active region is sandwiched between 100 nm thick lattice-matched $InGa_{0.882}As_{0.249}P$ separate confinement heterostructure layer. The waveguide core is later covered with ~0.8 μm and ~1.7 μm thick n- and p-type InP cladding layers with Si and Zn dopant, with doping concentration varying from $1 \times 10^{18} - 2 \times 10^{18}$ cm^{-3} and $5 \times 10^{17} - 5 \times 10^{18}$ cm^{-3}, respectively. The cladding layers are lattice-matched to the n-doped InP substrate and the metal-oxide chemical vapor deposition (MOCVD) grown device structure is completed by a 100 nm thick highly doped ($>1.5 \times 10^{19}$ cm^{-3}) $InGa_{0.533}As$ contact layer. The SLD devices are fabricated utilizing the standard fabrication process with 7° tilted ridge-waveguides with respect to the normal of the device facets. The 2 μm ridge-width SLDs are later cleaved to 1.0 mm length with both facets coated with AR coating before electrical characterization. For photoluminescence (PL) measurements, the un-fabricated full device structure is utilized and illuminated with 980 nm laser excitation source to measure the room temperature excitation power dependent PL. Several fabricated SLD devices were tested using both, pulsed mode (0.5 μs current pulse width and 0.01% duty cycle) and continuous wave (CW) operation, and under thermo-electric cooling. For emission spectra measurement, the optical power of the SLDs is butt-coupled into either a lensed multimode fiber which is connected to an optical spectrum analyzer pre-set at 1.0 nm resolution, or a wedge single-mode fiber with fine 0.1 nm resolution.

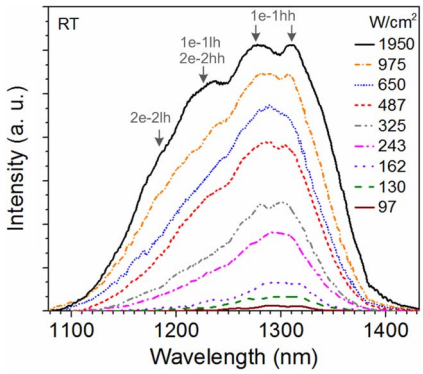

Fig. 1. Room temperature photoluminescence measurement from the full SLD device structure as a function of excitation power density. A PL linewidth of ∼185 nm is measured at 1950 W/cm^2 excitation power density.

3. Results and Discussion

Room temperature PL results of the SLD device structure under different excitation power density values is presented in Fig. 1. Two emission peaks at ∼1310 nm and ∼1276 nm are visible at high excitation density of $>$ 975 W/cm^2 which persists even at low excitation power of 97 W/cm^2. However, the two peaks are found to merge and later separate out with increasing excitation power density, thus indicating a comparable radiative recombination from the same QW transition state. We attribute these emission peaks to the recombination at GS e-hh (1e-1hh) state within the QWs and the bimodal behavior to the 1e-1hh state inhomogeneity across the MQWs. This is due in part to the composition and thickness fluctuation during growth and primarily to the variation in the built-in compressive strain that each succeeding QW experiences, leading to broadening of the 1e-1hh optical transitions [9], [21]. The emission hump at ∼1235 nm at high excitation power density of 1950 W/cm^2 again suggests bimodal peaks. In fact the evolution of the PL around this wavelength with increasing excitation power density show the hump composed of superposition of two emission peaks. Furthermore, a weak emission also appear at ∼1185 nm under excitation power density of $>$ 325 W/cm^2. These short wavelength emission humps and shoulders indicate the existence of ES emission in the MQW system. Therefore, we ascribe the emission at ∼1235 nm primarily to the ES e-hh (2e-2hh) transition states and partly to the GS e-lh (1e-1lh) recombination [21]. The latter transition state is possible in our compressively-strained MQW system which separates the 1e-1hh and 1e-1lh recombination, thus contributing to the inhomogeneity of the active region [9]. We attribute the shortest emission shoulder at ∼1185 nm to the emission from ES e-lh (2e-2lh) radiative transition which is found to be weak. In general, the collective emission from the dispersive GS and ES states, with each representing e-hh and e-lh recombination, respectively, contributed to the inhomogeneous broadening of our MQW active region system. Comparable emission intensities among the GS and ES emissions (∼0.7 dB difference between 1e-1hh and 2e-2hh) lead to an ultra-broad PL linewidth (full-width-at-half-maximum) of ∼185 nm (144 meV) at 1950 W/cm^2. Such a broad and fairly flat-topped PL profile shows the effectiveness of our device design for realization of broadband devices such as broadband lasers, semiconductor optical amplifiers, and SLDs.

Fig. 2(a) depicts the room temperature output power-current-voltage $(L-I-V)$ characteristic of our SLD (SLD1). The device exhibited a series resistance and a turn-on voltage of ∼1.1 V and 2–3 Ω, respectively. A super-linear characteristic is evident with total measured output power (2 facets, assuming identical facets reflectivity) of $>$ 70 mW. The corresponding ASE spectra at different pulsed current injection are shown in Fig. 2(b). An ultra-broad and flat-top emission profile is apparent with −3dB bandwidth $>$ 100 nm for injection current $\geq$ 0.1 A and reaching a maximum of 125 nm at 1.0 A. The summary of SLD characteristics as a function of pulsed current injection, at room temperature, is shown in Fig. 3(a). The central emission

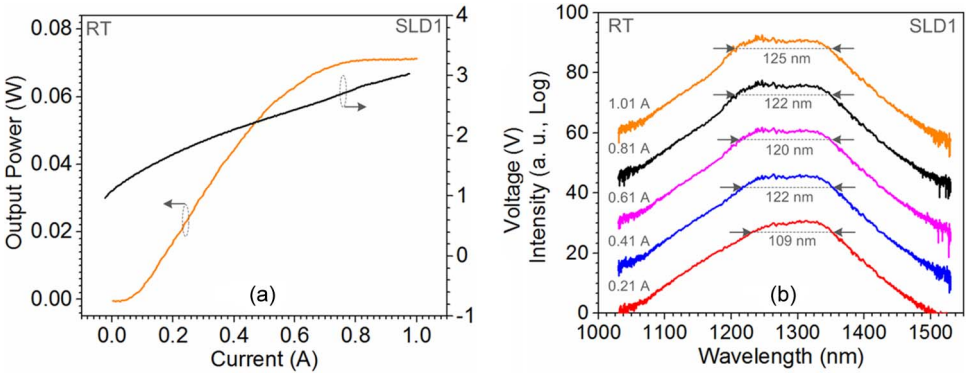

Fig. 2. (a) Room temperature $L-I-V$ characteristics of 7° tilted, AR coated, ridge waveguide 2 × 1000 μm^2 SLD1 device under pulsed current operation. The corresponding measured (b) emission spectra as a function of pulsed current injection. The −3 dB bandwidth at each injection current is shown in (b). The emission spectra in (b) are vertically offset for clarity.

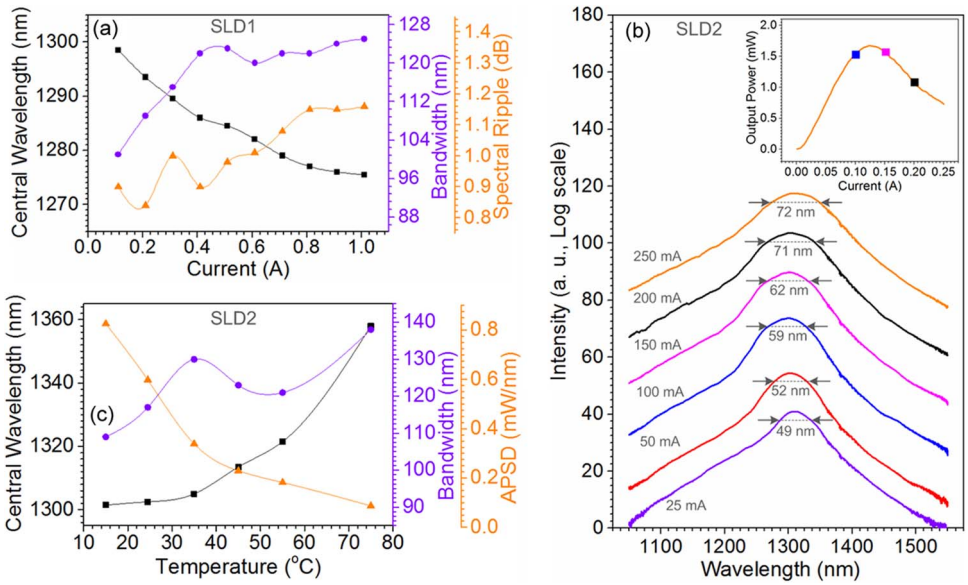

Fig. 3. (a) Effect of pulsed current injection on SLD1 device's central emission wavelength, emission bandwidth, and spectral ripple at room temperature. (b) Room temperature $L-I$ characteristics under CW current operation (inset), and emission spectra as a function of current injection, measured on SLD2 device. (c) Summarized changes in central emission wavelength, emission bandwidth, and APSD, with sub-mount temperature, of SLD2 device. The spectral ripple in (a) is measured within 10 nm wavelength span from the central emission wavelength and with an error margin of ±0.5 dB for > 0.2 A pulsed current injection. The solid lines in (a) and (c) are a guide to the eye, and the emission spectra in (b) are vertically offset for clarity.

wavelength (calculated by identifying the central wavelength at −3dB bandwidth) varied from ∼1300 nm to ∼1275 nm with increasing injection while the calculated PBP and average power spectral density (APSD) at 1.0 A are 8750 mWnm and 0.56 mW/nm, respectively. The device displayed a coherence length in air of 11.5 μm (0.88 times ratio of central wavelength square and −3dB bandwidth) and maximum external quantum efficiency (EQE) and WPE of 11.7% and 5.2%, respectively, which are reasonable values in SLD domain [5]. The spectral ripple, measured within 10 nm span from the central emission wavelength, is also plotted in Fig. 3(a). The ripple stayed below 1.0 ± 0.5 dB up to a pulsed current injection of 0.5 A and later increased to 1.2 ± 0.5 dB. In general, the spectral ripples using tilted configuration SLDs based on QW

active region are expected to show high values owing to the possibility of device operation reaching the onset of lasing because of the high modal gain of QW nanostructures [7].

This achievement of SLD performance is a result of active region engineering to obtain simultaneous and comparable emission from different QW transition states of the MQW system. Notice in Fig. 2(b) that during the low current injection, the longer wavelength emission near $\sim$1315 nm dominates compared to the shorter wavelength emission near $\sim$1240 nm. This is ascribed to the state filling and recombination of lower energy 1e-1hh transitions by the carriers first resulting in domination of ASE at $\sim$1315 nm [17]. However, the difference in the ASE level when compared to the emission from higher energy 1e-1lh and 2e-2hh states, corresponding to emission near $\sim$1240 nm, is mere $\sim$4.0 dB at 0.11 A (not shown). This value reduced considerably to $\sim$2.0 dB at 0.31 A, and eventually becomes negligible at 0.41 A (i.e., $<$ 0.5 dB), thus providing a flat-topped emission beyond this current value with comparable emission from both the dominating QW states. This observation is a direct effect of 1e-1hh energy level saturation because of completely filled density of states and therefore carriers occupying the next available higher energy level (1e-1lh and 2e-2hh) with increasing current injection, thus contributing to the increase in ASE at shorter wavelengths [12]. This phenomenon increases the emission bandwidth and inherently blue shifts the central emission wavelength, as summarized in Fig. 3(a). Moreover, it is worth mentioning that the device demonstrated an emission bandwidth of $>$ 100 nm for entire current range of $>$ 0.11 A, thus showing the effectiveness of the device design.

Fig. 3(b) shows the SLD performance under CW operation, measured from another device SLD2 which underwent identical fabrication and AR coating process (same batch) besides exhibiting similar pulsed $L-I-V$ and spectral characteristics, as that of SLD1. A total output power of $>$1.6 mW is measured at $\sim$0.12 A current injection with corresponding measured bandwidth of $\sim$60 nm. This is the maximum emission bandwidth measured from our device before power roll-off. A weak super-linear characteristic is visible in the inset of Fig. 3(b) with device reaching ASE regime within $\sim$20 mA of CW injection. The central emission wavelength is observed to be at $\sim$1310 nm under low injection of 25 mA which blue shift to $\sim$1296 nm at 0.12 A along with $\sim$13 nm increase in the $-$3dB bandwidth. This again dictates the dominance of GS 1e-1hh transition state under this mode of current operation. On comparing the CW characteristics with pulsed operation (Fig. 2), a different behavior in carrier emission process within the MQW active region is observed. An additional junction heating phenomenon under CW operation might have altered the carrier distribution among the QWs due to shallow conduction band offset and hence the way radiative recombination occurs in the inherent MQW inhomogeneous system [10], [22]. The device showed a red-shift in the emission wavelength and increase in the bandwidth by $\sim$10 nm (i.e., $\sim$72 nm) beyond 0.12 A with reduction in optical power because of excessive device heating. It is to be noted that our device structure and material quality is un-optimized and hence a substantial difference between the CW and pulsed operation is obvious.

In order to investigate the SLD performance at elevated temperatures, SLD2 is tested at various temperatures under pulsed operation. The results are shown in Fig. 3(c). The device performance degraded substantially on varying the temperature from 15 °C to 45 °C with the APSD reducing from 0.8 mW/nm at 15 °C to 0.2 mW/nm at 45 °C and eventually to 0.08 mW/nm at 75 °C. This is accompanied by an appreciable redshift in the central emission wavelength from $\sim$1300 nm at 15 °C to $\sim$1313 nm at 45 °C and eventually to $\sim$1355 mW/nm at 75 °C. The drastic decrease in the optical power with increasing temperature is attributed to the shallow conduction band offsets of InGaAsP material system, thus favoring carrier spill over with increasing temperature rather than radiatively recombining within the QW (weak carrier confinement) [23]. Note that the emission bandwidth shows a sigmoidal behavior accompanied by reduction in the signal-to-noise ratio with increasing temperature, indicating competition between the QW energy states for eventual domination. In fact we observed multiple emission peaks in the ASE spectra at elevated temperatures ($>$ 35 °C) with one of them dominating (and also found it to be a function of injection current), indicating non-uniform distribution of carriers among the QWs at high temperature [21], [22]. We attribute this complex temperature dependent ASE emission and red shift in the central emission wavelength to the collective phenomena such as junction

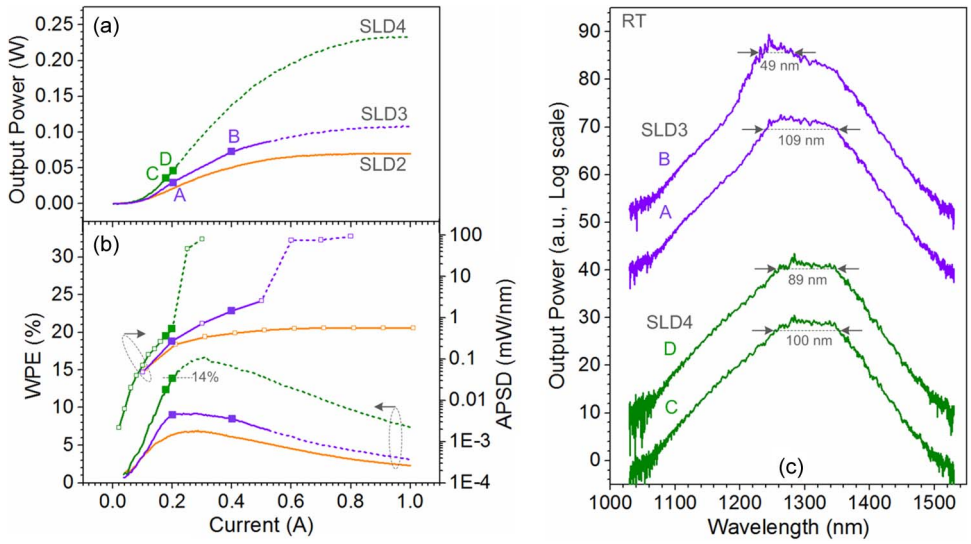

Fig. 4. Room temperature (a) $L-I$ characteristics of 7° tilted, AR coated, ridge waveguide $2 \times 1000\ \mu m^2$ SLD2, SLD3, and SLD4 devices under pulsed current operation, and the corresponding (b) APSD and WPE as a function of pulsed current injection. (c) Emission spectra of SLD3 and SLD4 devices at two pulsed current injection values (A = D = 0.2 A, B = 0.4 A, and C = 0.18 A). The solid and dashed lines in (a) and (b) corresponds to the ASE and stimulated emission regimes, respectively. Note that the alteration in the facets reflectivity resulted in different device performance with WPE reaching as high as 14%.

heating, phonon-assisted tunneling, optical activation, etc., occurring simultaneously in the MQW system [24].

We selected two more devices (SLD3 and SLD4) from the same batch that underwent identical fabrication and AR coating process, and plotted their room temperature pulsed $L-I$ characteristics in Fig. 4(a), besides SLD2 results. The respective APSD, WPE values, and emission spectra are plotted in Figs. 4(b) and (c). A substantial increase in the output power from SLD3 and SLD4 with values reaching ~31 mW with PBP of 3380 mWnm (at 0.2 A) and ~37 mW with PBP of 5120 mWnm (at 0.18 A), are observed, when compared to ~22 mW with PBP of 2398 mWnm from SLD2 (at 0.2 A), under pulsed injection. This corresponds to approximately 1.5–2.0 times increase in PBP value compared to SLD2, with SLD3 exhibiting output power in excess of 80 mW at $\geq$ 0.45 A. In general, an emission bandwidth of at least 100 nm and APSD $>$ 0.4 mW/nm are demonstrated by both SLD3 and SLD4 devices. Additional attractive feature worth mentioning about these devices is the significant increase in their efficiencies, plotted in Fig. 4(b). An EQE (not shown here) and WPE in excess of 13.5% and 7%, 18.5% and 9%, 24% and 14%, are observed from SLD2, SLD3, and SLD4, respectively. The latter device efficiencies are double in value when compared to the former one, and comparable to the achievements at other wavelengths (WPEs of 28% [25] at 1500 nm and 16% [2] at 980 nm).

The above difference in the performance of SLD devices is a result of alteration in AR coating thickness, thus modifying the reflectivity value of the facets. We postulate that the facets reflectivity of SLD2 $<$ SLD3 $<$ SLD4, thus allowing higher level of ASE to undergo multiple-pass amplification in SLD4 compared to SLD2 and hence increased optical power. It is noted that the possibility of achieving lasing condition is higher in this SLD configuration; therefore, the device is required to operate below the onset of lasing threshold to maintain large PBP. This is a potential method to improve the performance by engineering the reflectivity (AR coating thickness) of the MQW SLD facets. In existing SLD literature, schemes for controlling the power [12] or wavelength [26] of the rear facet optical feedback signal with front facet AR coated, has been demonstrated to increase the SLD power and engineer the ASE spectra profile, respectively, employing bulky optical components, in general. While in the stimulated emission regime, gain flattening coating on asymmetric MQW InGaAsP/InP laser was demonstrated that allowed

achievement of laser operation over wider spectral range [27]. Therefore, the approach of controlling the reflectivity of both facets, without any external optics, will allow higher power level to be achieved while preserving the SLD performance, due to multiple-pass ASE amplification, compared to the reported double-pass amplification schemes.

4. Conclusion

We demonstrated a high-power and ultrawide bandwidth InGaAsP/InP MQW SLD. Room temperature PL linewidth of more than 180 nm from the device structure affirms the inhomogeneous nature of the MQW active region. The device exhibited a flat-top emission bandwidth of 125 nm and APSD $\sim$0.56 mW/nm with low spectral ripple $\leq 1.2 \pm 0.5$ dB, thus asserting our achievement in designing inhomogeneous active region with comparable emission from different QW transition states. Furthermore, WPE as high as 14% is achieved from this batch of devices thus paving way for possible facets reflectivity engineering approach in obtaining high efficiency and PBP SLD devices. Our current demonstration of high-efficiency, high-power, flat-top and broadband SLD may shift the paradigm, which is dominated by InAs/GaAs self-assembled Qdots, back to MQW system.

References

[1] T. Ko *et al.*, "Ultrahigh resolution optical coherence tomography imaging with a broadband superluminescent diode light source," *Opt. Exp.*, vol. 12, no. 10, pp. 2112–2119, May 2004.
[2] L. Burrow, F. Causa, and J. Sarma, "1.3-W ripple-free superluminescent diode," *IEEE Photon. Technol. Lett.*, vol. 17, no. 10, pp. 2035–2037, Oct. 2005.
[3] S. Haffouz, P. Barrios, R. Normandin, D. Poitras, and Z. Lu, "Ultrawide-bandwidth, superluminescent light-emitting diodes using InAs quantum dots of tuned height," *Opt. Lett.*, vol. 37, no. 6, pp. 1103–1105, Mar. 2012.
[4] K. Zhou *et al.*, "Quantum dot selective area intermixing for broadband light sources," *Opt. Exp.*, vol. 20, no. 24, pp. 26950–26957, Nov. 2012.
[5] Z. Zhang, R. Hogg, X. Lv, and Z. Wang, "Self-assembled quantum-dot superluminescent light-emitting diodes," *Adv. Opt. Photon.*, vol. 2, no. 2, pp. 201–228, Jun. 2010.
[6] H. S. Djie *et al.*, "InGaAs/GaAs quantum-dot superluminescent diode for optical sensor and imaging," *IEEE Sensors Journal*, vol. 7, no. 2, pp. 251–257, Feb. 2007.
[7] J. Wang, M. J. Hamp, and D. T. Cassidy, "Design considerations for asymmetric multiple quantum well broad spectral width superluminescent diodes," *IEEE J. Quantum Electron.*, vol. 44, no. 12, pp. 1256–1262, Dec. 2008.
[8] O. Mikami, H. Yasaka, and Y. Noguchi, "Broader spectral width InGaAsP stacked active layer superluminescent diodes," *Appl. Phys. Lett.*, vol. 56, no. 11, pp. 987–989, Mar. 1990.
[9] H. Ma, S. Chen, X. Yi, G. Zhu, and J. Jin, "High power polarization-insensitive 1.3 μm InGaAsP-InP quantum-well superluminescent emission diodes grown by MOVPE," *Semicond. Sci. Technol.*, vol. 19, no. 7, pp. 823–827, 2004.
[10] L. Fu *et al.*, "Design and realization of high-power ripple-free superluminescent diodes at 1300 nm," *IEEE J. Quantum Electron.*, vol. 40, no. 9, pp. 1270–1274, Sep. 2004.
[11] M. Sugo, Y. Shibata, H. Kamioka, M. Yamamoto, and Y. Tohmori, "High-power ($>$ 50 mW) and wideband ($>$ 50 nm) 1.3 μm super-luminescent diodes," *Electron. Lett.*, vol. 41, no. 8, pp. 500–501, Apr. 2005.
[12] M. Faugeron *et al.*, "Wide optical bandwidth and high output power superluminescent diode covering C and L band," *IEEE Photon. Technol. Lett.*, vol. 26, no. 8, pp. 841–844, Apr. 2014.
[13] M. Khan, T. Ng, and B. Ooi, "High performance 1.55 μm superluminescent diode based on broad gain InAs/InGaAlAs/InP quantum dash active region," *IEEE Photon. J.*, vol. 6, no. 4, Aug. 2014, Art. ID. 1600108.
[14] B. S. Ooi *et al.*, "Quantum dashes on InP substrate for broadband emitter applications," *IEEE J. Sel. Top. Quantum Electron.*, vol. 14, no. 4, pp. 1230–1238, Jul./Aug. 2008.
[15] S. Chen *et al.*, "Broad bandwidth emission from hybrid QW/QD structures," in *Proc. Conf. Lasers Electro-Opt./Pac. Rim*, 2013, p. pp. 1–2, WK1_3.
[16] T. R. Chen *et al.*, "Quantum well superluminescent diode with very wide emission spectrum," *Appl. Phys. Lett.*, vol. 56, no. 14, pp. 1345–1346, Apr. 1990.
[17] C.-F. Lin, B.-R. Wu, L.-W. Laih, and T.-T. Shih, "Sequence influence of nonidentical InGaAsP quantum wells on broadband characteristics of semiconductor optical amplifiers-superluminescent diodes," *Opt. Lett.*, vol. 26, no. 14, pp. 1099–1101, Jul. 2001.
[18] [Online]. Available: http://www.covega.com/Products/pdfs/SLD%201018%20XL%20Rev%20A.pdf
[19] [Online]. Available: http://www.denselight.com/downloads/SLED/DL-CS3504A_RevA.pdf
[20] [Online]. Available: http://www.thorlabs.de/thorcat/19400/SLD1018S-SpecSheet.pdf
[21] H. Carrère *et al.*, "Large optical bandwidth and polarization insensitive semiconductor optical amplifiers using strained InGaAsP quantum wells," *Appl. Phys. Lett.*, vol. 97, no. 12, Sep. 2010, Art. ID. 121101.
[22] H. Wang, A. D. Vandermeer, and D. T. Cassidy, "Carrier distribution and its dependence on barrier thickness in InGaAsP/InP asymmetric multiple quantum well lasers," *J. Appl. Phys.*, vol. 100, no. 9, Nov. 2006, Art. ID. 093104.

[23] S. Seki, H. Oohasi, H. Sugiura, T. Hirono, and K. Yokoyama, "Dominant mechanisms for the temperature sensitivity of 1.3 μm InP-based strained-layer multiple-quantum-well lasers," *Appl. Phys. Lett.*, vol. 67, no. 8, pp. 1054–1056, Aug. 1995.
[24] C. Rejeb, R. Maciejko, D. Morris, and T. Makino, "Carrier dynamics in InGaAsP MQW laser structures," in *Proc. Int. Conf. Appl. Photon. Technol.*, 1998, pp. 1065–1070.
[25] W. Li, R. Ronkko, A. Rydefalk, P. Poyhonen, and M. Pessa, "Superluminescent diodes at 1.55 μm based on quantum-well and quantum-dot active regions," in *Proc. Integr. Optoelectron. Dev.*, 2005, pp. 116–121.
[26] M. Blazek *et al.*, "Coherence function control of quantum dot superluminescent light emitting diodes by frequency selective optical feedback," *Opt. Exp.*, vol. 17, no. 16, pp. 13 365–13 372, Aug. 2009.
[27] X. Tan, D. T. Cassidy, and P. Mascher, "Gain flattening coatings for improved spectral performance of asymmetric multiple quantum well lasers," *Appl. Opt.*, vol. 50, no. 6, pp. 975–980, Feb. 2011.